IEEE Access
Multidisciplinary | Rapid Review | Open Access Journal

Received April 22, 2019, accepted May 21, 2019, date of publication June 4, 2019, date of current version June 17, 2019.

Digital Object Identifier 10.1109/ACCESS.2019.2920291

W-Band and D-Band Traveling-Wave Tube Circuits Fabricated by 3D Printing

ALAN M. COOK, (Senior Member, IEEE), COLIN D. JOYE, (Senior Member, IEEE), AND JEFFREY P. CALAME, (Fellow, IEEE)
Naval Research Laboratory, Washington, DC 20375, USA

Corresponding author: Alan M. Cook (alan.cook@nrl.navy.mil)

This work was supported by the U.S. Office of Naval Research.

ABSTRACT We present the fabrication and electromagnetic testing of serpentine waveguide traveling-wave tube amplifier circuits operating in the *W*-band (75–110 GHz) and *D*-band (110–170 GHz) frequency ranges. The circuit structures were fabricated in a split-block configuration in a photopolymer material using a commercial digital light processing (DLP) 3D printer and, subsequently, covered with a conducting layer by Au sputtering and Cu electroplating. Two-port S-parameter measurements of the *W*-band circuit demonstrate a transmission band from ∼87-104 GHz, with a 26.7-dB return loss and a 0.55-dB insertion loss measured at 95 GHz. The *D*-band circuit demonstrates a transmission band from ∼139 to 145 GHz, with a 21.5-dB return loss and a 2.4-dB insertion loss measured at 140 GHz.

INDEX TERMS Electron tubes, microfabrication, millimeter wave circuits, three-dimensional printing.

I. INTRODUCTION

Additive manufacturing and three-dimensional (3D) printing technology presents opportunities for fabrication of electromagnetic structures such as antennas and waveguides operating at high frequencies, in the millimeter-wave (mmW) and upper-mmW range [1]–[3]. The use of 3D-printing-based fabrication methods for microwave/mmW components such as filters or traveling-wave amplifier circuits, which require precise wavelength dispersion properties to operate with the designed phase and frequency response across a wide bandwidth, is limited by machine constraints such as build resolution and build material properties. For example, traveling-wave circuits operating in the W-band frequency range (75-110 GHz) have critical feature sizes on the order of 200 μm, which nominally require a 3D volume pixel (''voxel'') size on the order of 20 μm to accurately represent. This limits the available build materials to those capable of fine resolution, which are further restricted to materials that have electrical conductivity or that can be plated [4]. Build materials are a key limiting factor in the achievable resolution due to the influence of material properties on the curing and dynamics of the material during the build process.

Upper-mmW components with complex geometries and good RF performance, including waveguide, magic tees, filters, and directional couplers, have been successfully demonstrated using some of the highest-resolution 3D printing technologies currently available [5]–[7]. This development could constitute a major advance for traveling-wave tube (TWT) vacuum electron devices, which incorporate a broadband traveling-wave circuit that interacts with a focused electron beam in vacuum to amplify millimeter waves, and which could benefit from the component integration, rapid fabrication/prototyping, and multi-material capabilities offered by additive manufacturing.

In this paper, we demonstrate high-precision fabrication of W-band and D-band serpentine waveguide traveling-wave circuits using a commercial 3D printer. This circuit type is characterized by a rectangular waveguide folding back and forth in 180-degree E-plane bends as seen in Fig. 1(a). The circuit operates in the fundamental $TE_{1,0}$ waveguide mode, with the electric field vector always parallel to the XY plane in the figure, where the waveguide broad wall extends along Z. A key application of this structure type is as an interaction circuit in upper-mmW TWT amplifiers [8]–[10]. For that reason, the structure includes a longitudinal round tunnel to allow an electron beam to pass through. We focus our study on the dimensional accuracy and electromagnetic properties of the as-fabricated structures, to evaluate the suitability of this fabrication technique for traveling-wave devices and passive components in the upper mmW frequency range.

The associate editor coordinating the review of this manuscript and approving it for publication was Vittorio Camarchia.

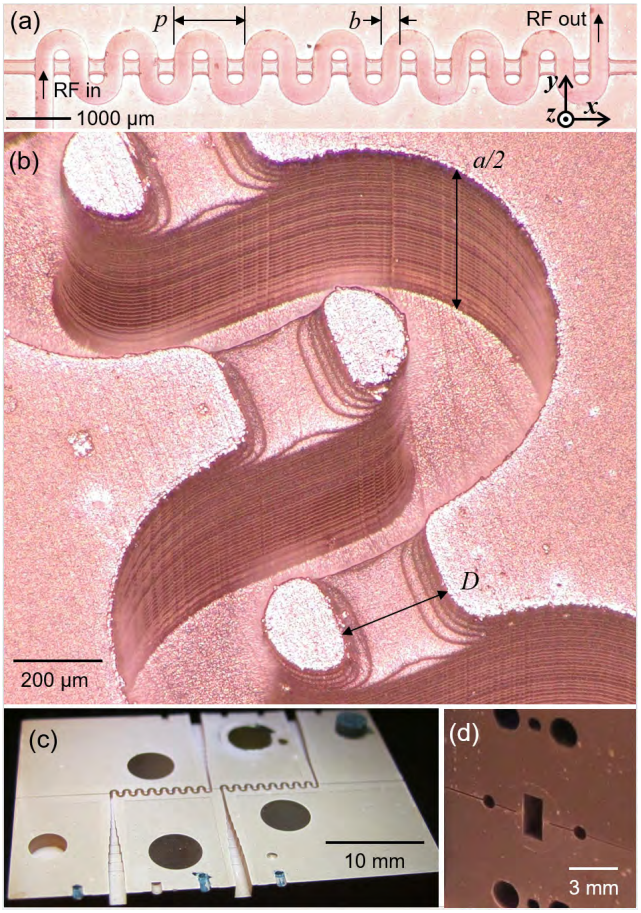

FIGURE 1. W-band serpentine waveguide traveling-wave circuit fabricated by 3D printer, after Cu electroplating. (a) Half of split-block circuit, top view. (b) Detail view of circuit; fine corrugations in waveguide wall due to 3D-printed layers are visible. (c) Bottom half of split block, containing two circuits, integrated waveguide transitions, and alignment holes. (d) WR10 waveguide opening when split block is assembled.

II. 3D-PRINTED CIRCUIT FABRICATION

To fabricate the circuits, we used a commercial vat photopolymerization 3D printer of the digital light processing (DLP) type [11], manufactured by EnvisionTEC, Inc., model "P4 Mini." The machine uses a digital projector to project 2D images in sequence into a tray of liquid photopolymer resin, building up a 3D model from 2D slices. The voxel size setting was 30 × 30 μm in XY and 25 μm layer thickness (Z). We used the proprietary off-the-shelf build material "HTM140 v2" (EnvisionTEC Inc.), a high-temperature molding material with nominal heat deflection temperature 140°C.

The circuits were built in two halves in a split-block configuration, to allow access to the inside of the waveguide structure for plating. The block design contains multiple circuits, integrated waveguide transitions, and features for alignment and assembly. Microscope images of one half of the split block of a W-band circuit are shown in Fig. 1(a-c). After being built on the 3D printer, the block was lapped on the split-plane faces to ensure precision flatness at the mechanical joint, coated with a thin conducting layer by Au sputtering, and DC-electroplated with Cu using a $CuSO_4$ solution [12]. The Cu layer is estimated to be 1-2 μm thick based on the process parameters, which is ∼5 times the RF skin depth at W-band, sufficient to provide high reflection in that frequency range [13]. The roughness of the plated surface at the waveguide bottom was measured to be $R_a \approx 400$ nm using a laser confocal microscope. Finally, the two halves were clamped together by stainless steel screws, using 3D-printed alignment dowel pins and holes for accurate registration. A single split-block assembly yielded two separate circuits that were independently tested. Fig. 1(d) shows the WR10 waveguide opening when the structure is assembled and ready for electromagnetic testing.

A. DIMENSIONAL ACCURACY AND PRECISION

To quantify the build accuracy and precision of the W-band circuits, we measured the characteristic critical dimensions at each circuit period using a digital optical measurement microscope, as labeled in Fig. 1(a,b): the longitudinal period p of the serpentine circuit; the narrow-wall width b and broad-wall height a of the waveguide; and the diameter D of the beam tunnel. Table 1 shows statistics compiled from these measurements, calculated across all four circuit halves except for waveguide height, which is calculated for the two complete circuit assemblies. We report the achieved accuracy as a percentage error between the mean value and the design value. We report the achieved precision as a percentage variation, computed as the standard deviation divided by the mean.

We observe excellent accuracy and precision in the period p, with error (variation) of 0.3% (0.2%). The period is a key dimension determining the wavelength dispersion in the circuit, and thus the RF performance of any device based on the circuit. Another critical dimension is the waveguide height a, which determines the cutoff frequency and affects

TABLE 1. Critical dimensions, As-fabricated.

Symbol	Dimension	Design value (μm)	Mean value as-fabricated (μm)	Accuracy relative to design (% error)	Precision (std. deviation rel. to mean) (% variation)
p	Serpentine period	1126	1123	0.3%	0.2%
b	Waveguide width	277	282	1.8%	2.8%
a	Waveguide height in Z	1766	1825	3.3%	0.8%
D	Beam tunnel diam.	230	232	0.9%	5.1%

Measured dimensions of fabricated W-band circuits, as labeled in Fig. 1(a,b), compared to ideal design values. Statistics are calculated across all four circuit halves except for waveguide height a, which is calculated for the two complete circuit assemblies.

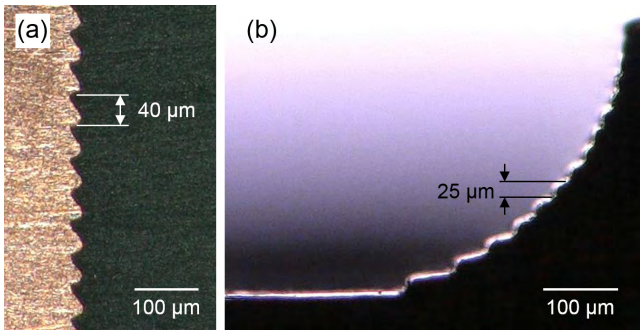

FIGURE 2. **(a) Example of corrugations in waveguide broad wall due to 3D-printed layers, when build layer thickness is set to 40 μm. (b) Stair-step artifacts in cylindrical shape, when layer thickness is set to 25 μm. In each photo, dark areas are 3D-printed material.**

TABLE 2. **Comparison between fabrication methods.**

	3D printed, Cu-plated (this paper)	3D-printed mold electro-forming [19]	CNC machine	UV-LIGA [10,12]
material	HTM140 v2, Cu-plated	Solid Cu	Solid Cu	Solid Cu
p variation	2.7 µm; (0.2%)	5 µm; (0.5%)	1.5 µm; (0.15%)	3 µm; (0.3%)
a variation	14.8 µm; (0.8%)	9 µm; (0.5%)	7 µm; (0.4%)	5 µm; (0.3%)

Comparison of achieved critical dimension precision between four circuit fabrication methods, reported as std. deviation (std. deviation rel. to mean).

the operating frequency band of the circuit. We observe reasonably low variation (0.8%) in a across the circuits, but significant average error from the design value (3.3%). This is partly due to stress in the 3D-printed material causing an observable smooth curvature deformation of the overall part, with a maximum displacement on the order of 2 printed layers (50 μm) in the Z direction across the ~40 mm-wide block. Other possible causes include imperfect lapping of the split-plane faces and inaccuracies in calibrating the Z-position of the 3D printer build plate. Dimensions b and D also show variation on the order of a few percent, possibly due to non-uniformity in the optical exposure intensity across the build area in the 3D printer. This may be addressed by exploring improved optical calibration techniques and corresponding compensation of the target dimensions; however, these dimensions are not critical to the RF performance of the circuit. The measured variation and error in b, D, and p amount to $\leq$5-10 μm (0.0002-.0004") in absolute value and are within an acceptable tolerance, comparable to the sub-.001" tolerances typical of precision CNC machining and previously reported TWT circuit microfabrication methods (Table 2).

B. LOW-RESOLUTION ARTIFACTS

The finite build resolution primarily manifests as a layered or "stair-stepping" appearance in vertical or sloped surfaces, respectively. Fig. 2(a) shows a cut side-view example of corrugations in a waveguide vertical wall created by stacked

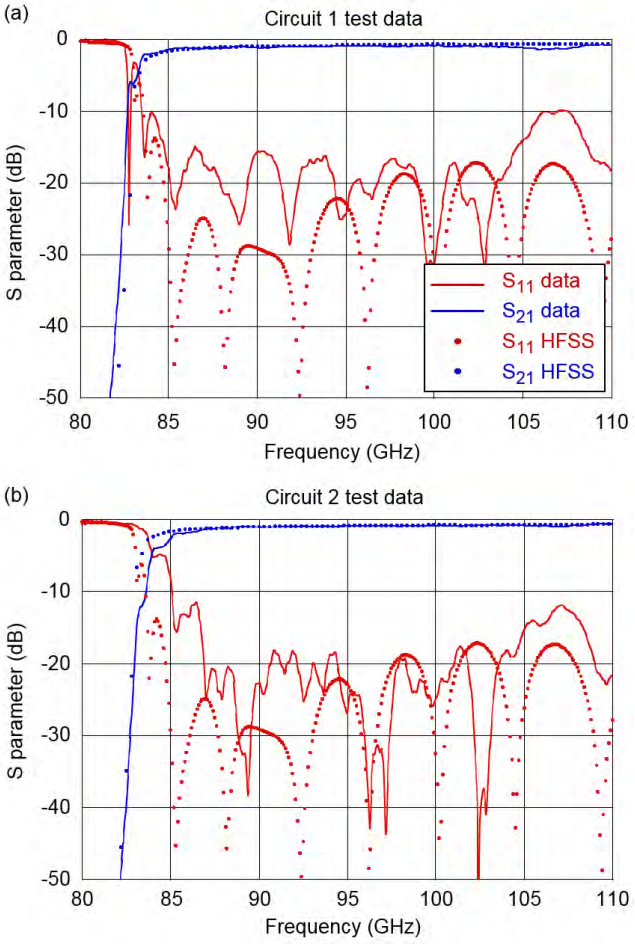

FIGURE 3. **S-parameters of (a) circuit 1 and (b) circuit 2, measured by vector network analyzer (solid lines); HFSS simulation (dots).**

3D-printed layers. In this example, the machine setting for layer thickness is 40 μm. Fig. 2(b) shows 25 μm layers evident in a cylindrical wall. Both photos are oriented such that the projected light exposure during printing is directed downward from the top of the page. The measured layer thickness is very close to the machine setting in both cases, indicating good repeatability of the build parameters. We observe that the voxel width in XY does not noticeably deform contoured shapes in the XY plane, such as the waveguide bend curves, at this scale. The resulting smooth contours and the effect of layering on the beam tunnel and waveguide walls are apparent in Fig 1(b).

III. ELECTROMAGNETIC TEST RESULTS

Figure 3 shows the two-port S-parameters of each of two W-band circuits, measured in the frequency range 75-110 GHz with a mmW vector network analyzer. The data are compared to a simulation using the 3D electromagnetic solver HFSS [14]. The simulation assumes smooth internal waveguide walls, not accounting for the corrugated nature of the 3D-printed layers; and a uniform waveguide height equal to the shallowest part of the measured waveguide, not accounting for stress-induced height variation. Each circuit

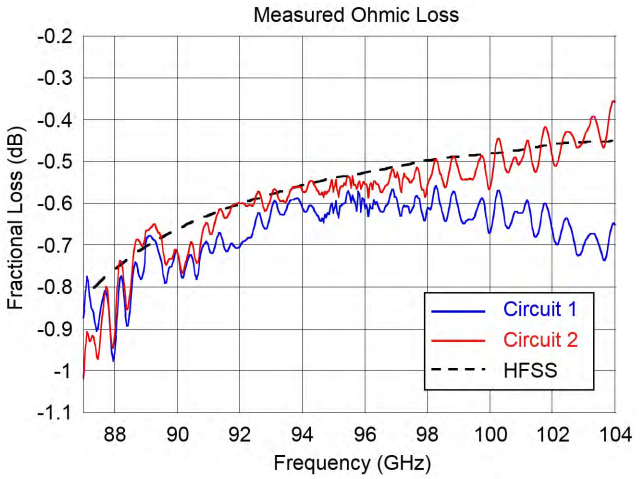

FIGURE 4. Measured ohmic loss of W-band circuits (solid lines); HFSS simulation of smooth-walled circuit using effective RF conductivity $5.8\text{x}10^7$ S/m (dashed line).

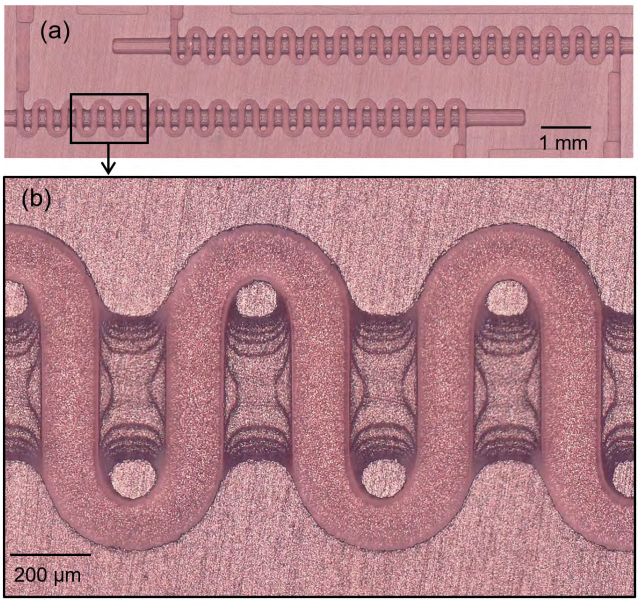

FIGURE 5. 140 GHz serpentine waveguide traveling-wave circuit fabricated by 3D printer, after Cu electroplating.

is compared to the same simulation. We observe good quantitative agreement in both S_{11} and S_{21} near the cutoff frequency $f_c \approx 82.5$ GHz in circuit 1 (Fig. 3(a)). Circuit 2 has better low-reflection performance in the passband, achieving approximately 18-20 dB return loss over the range 87-104 GHz (Fig. 3 (b)), and having good quantitative agreement with the simulation above ~95 GHz. We measure 26.7 dB return loss and 0.55 dB insertion loss at 95 GHz in circuit 2.

The insertion loss of the circuit is an important metric for establishing the utility of 3D-printed circuits in practical devices. Fig. 4 shows the fractional dissipated power calculated from the complex S-parameter data in the passband 87-104 GHz. The measured loss is compared to HFSS simulations of a smooth-walled circuit assuming an effective RF conductivity of the Cu-plated surface equal to the DC

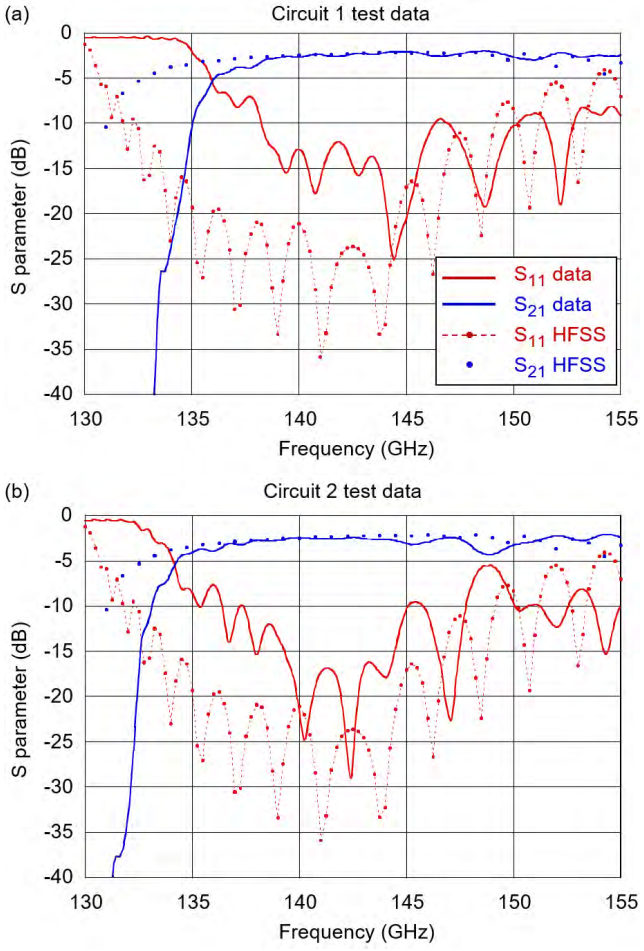

FIGURE 6. S-parameters of 140 GHz circuits, measured by vector network analyzer (solid lines); HFSS simulation (dots).

value of bulk Cu ($5.8\text{x}10^7$ S/m). The excellent agreement between data and simulation across the passband indicates that the observed low-resolution artifacts such as the corrugated waveguide walls do not significantly affect the insertion loss of the circuit at this scale, consistent with previous results in upper-mmW straight rectangular waveguide [15]. The loss data are corrected for 0.3 dB insertion loss of the connecting waveguides, measured at mid-band. The increased loss observed in circuit 1 at higher frequency may be due to a spurious reflection band near 107 GHz that is more pronounced in circuit 1 (Fig. 3(a)), commonly observed in serpentine-waveguide type circuits due to the bi-periodic nature of small fabrication errors [9].

IV. D-BAND CIRCUIT RESULTS

We fabricated D-band (110-170 GHz) circuits using the process described in Section II. The circuits were designed for operation near 140 GHz. Microscope images of one half of the split block of the circuit are shown in Fig. 5, after Cu electroplating and prior to split block assembly. Fig. 6 shows the measured S-parameters of two D-band circuits fabricated on the same block, both compared to the same HFSS

simulation of the ideal circuit design. It is notable that the measured cutoff frequency and passband are shifted up in frequency significantly compared to the simulation. This is presumed due to the stress-induced curvature of the 3D-printed part and subsequent lapping causing reduced waveguide height, and is a more pronounced effect than we observed at lower frequencies in W-band. Both circuits demonstrate a passband approximately 139-145 GHz. Circuit 2 has better low-reflection performance in the passband, achieving approximately 15-20 dB return loss over the range 139-144 GHz (Fig. 6 (b)). We measure 21.5 dB return loss and 2.4 dB insertion loss at 140 GHz in circuit 2. While the measured insertion loss is significantly higher than at W-band, it is in excellent agreement with simulation. Increased loss is expected due to lower effective electrical conductivity at higher frequencies.

V. CONCLUSION

These results show that high-resolution vat photo-polymerization 3D printing is capable of the accuracy and precision required to realize functional traveling-wave circuits in the W-band and D-band frequency ranges. Although build resolution effects are visible in the finished parts, the measured frequency response and insertion loss are comparable to that of ideal smooth-wall circuit simulations, indicating that 3D-printed circuits are capable of excellent RF performance at upper-mmW frequencies well above 100 GHz.

Material properties of the cured photopolymer are a primary concern for integration of a 3D-printed circuit into a TWT device. One limitation is vacuum compatibility, which is critical in vacuum electron devices where outgassing could potentially poison electron beam emission processes and produce unacceptably high base pressure. We performed a preliminary test with a small HTM140 v2 3D-printed cylinder, 3.175 mm in diameter and 2.4 mm in height, placed in a vacuum chamber. Pressure $5.0\text{x}10^{-9}$ Torr was reached at 24 hours after baking at 110°C for two hours, providing an initial indication of good vacuum compatibility for small parts made from this material [16], [17]. Another important consideration is the typically low thermal conductivity of plastic materials, which would not allow efficient cooling of a device operating at high average power. The thin metal coating might also suffer erosion from stray electron beam scraping, or allow electrons to pass into the underlying polymer if the electron beam stopping depth exceeds the coating thickness, causing additional outgassing.

Another limiting factor is the high processing temperatures that are typically used to seal the vacuum envelope of a TWT device by brazing (>700 °C) and to bake out the evacuated assembly to improve the pressure (∼500°C), which are well in excess of the melting point of 3D-printed polymer material. A vacuum device incorporating this material would need to be engineered to use welds or resealable flanges for the final vacuum seals, external to the 3D-printed part, and would need to limit the bakeout temperature to <140 °C (material-dependent).

While significant further work is needed to assess these materials issues, the favorable RF test results presented here show that circuits fabricated by DLP 3D printing followed by electroplating likely have immediate utility in low-power upper-mmW passive component applications, and potentially in active vacuum electron devices operating at extremely low average power if electron beam interception is minimal. Such a device was demonstrated in a high-power L-band magnetron with a 3D-printed, Cu-plated anode, operating in pulses less than 50 ns in duration [18]. More generally, these RF tests show that low-resolution geometric artifacts such as stair-stepping and layering, which are a common trait of 3D-printed parts in various materials including metals and ceramics, can be compatible with excellent RF performance in the upper-mmW regime. This indicates that additive manufacturing methods that build directly in metal or use 3D-printed plastic as a mold for metal [19] could be used to create low-loss mmW traveling-wave circuits that do not suffer from limitations imposed by plastic materials and that could be more readily integrated into a practical vacuum electron device.

REFERENCES

[1] M. Abbasi and D. S. Ricketts, "W-Band corrugated and non-corrugated conical horn antennas using Stereolithography 3D-printing technology," in *Proc. Asia–Pacific Microw. Conf. (APMC)*, New Delhi, India, Dec. 2016, pp. 1–3. doi: 10.1109/APMC.2016.7931300.

[2] B. Zhang, Z. Zhan, Y. Cao, H. Gulan, P. Linnér, J. Sun, T. Zwick, and H. Zirath, "Metallic 3-D printed antennas for millimeter- and submillimeter wave applications," *IEEE Trans. THz Sci. Technol.*, vol. 6, no. 4, pp. 592–600, Jul. 2016. doi: 10.1109/TTHZ.2016.2562508.

[3] M. D'Auria, W. J. Otter, J. Hazell, B. T. W. Gillatt, C. Long-Collins, N. M. Ridler, and S. Lucyszyn, "3-D printed metal-pipe rectangular waveguides," *IEEE Trans. Compon. Packag. Manuf. Technol.*, vol. 5, no. 9, pp. 1339–1349, Sep. 2015. doi: 10.1109/TCPMT.2015.2462130.

[4] J. Shen, M. Aiken, C. Ladd, M. Dickey, and D. Ricketts, "A simple electroless plating solution for 3D printed microwave components," in *Proc. Asia–Pacific Microw. Conf. (APMC)*, New Delhi, India, Dec. 201, pp. 1–4. doi: 10.1109/APMC.2016.7931434.

[5] J. Shen and D. S. Ricketts, "Additive manufacturing of complex millimeter-wave waveguides structures using digital light processing," *IEEE Trans. Microw. Theory Techn.*, vol. 67, no. 3, pp. 883–895, Mar. 2019. doi: 10.1109/TMTT.2018.2889452.

[6] X. Shang, P. Penchev, C. Guo, M. J. Lancaster, S. Dimov, Y. Dong, M. Favre, M. Billod, and E. de Rijk, "W-band waveguide filters fabricated by laser micromachining and 3-D printing," *IEEE Trans. Microw. Theory Techn.*, vol. 64, no. 8, pp. 2572–2580, Aug. 2016. doi: 10.1109/TMTT.2016.2574839.

[7] S. Verploegh, M. Coffey, E. Grossman, and Z. Popović, "Properties of 50–110-GHz waveguide components fabricated by metal additive manufacturing," *IEEE Trans. Microw. Theory Techn.*, vol. 65, no. 12, pp. 5144–5153, Dec. 2017. doi: 10.1109/TMTT.2017.2771446.

[8] G. Dohler, D. Gagne, D. Gallagher, and R. Moats, "Serpentine waveguide TWT," in *IEDM Tech. Dig.*, Dec. 1987, pp. 485–488. doi: 10.1109/IEDM.1987.191465.

[9] K. T. Nguyen, A. N. Vlasov, L. Ludeking, C. D. Joye, A. M. Cook, J. P. Calame, J. A. Pasour, D. E. Pershing, E. L. Wright, S. J. Cooke, B. Levush, D. K. Abe, D. P. Chernin, and I. A. Chernyavskiy, "Design methodology and experimental verification of serpentine/folded-waveguide TWTs," *IEEE Trans. Electron Devices*, vol. 61, no. 6, pp. 1679–1686, Jun. 2014. doi: 10.1109/TED.2014.2303711.

[10] C. D. Joye, A. M. Cook, J. P. Calame, D. K. Abe, A. N. Vlasov, I. A. Chernyavskiy, K. T. Nguyen, E. L. Wright, D. E. Pershing, T. Kimura, M. Hyttinen, and B. Levush, "Demonstration of a high power, wideband 220-GHz traveling wave amplifier fabricated by UV-LIGA," *IEEE Trans. Electron Devices*, vol. 61, no. 6, pp. 1672–1678, Jun. 2014. doi: 10.1109/TED.2014.2300014.

[11] S. C. Ligon, R. Liska, J. Stampfl, M. Gurr, and R. Mülhaupt, "Polymers for 3D printing and customized additive manufacturing," *Chem. Rev.*, vol. 117, pp. 10212–10290, Jul. 2017. doi: 10.1021/acs.chemrev.7b00074.

[12] C. D. Joye, J. P. Calame, M. Garven, and B. Levush, "UV-LIGA microfabrication of 220 GHz sheet beam amplifier gratings with SU-8 photoresists," *J. Micromech. Microeng.*, vol. 20, no. 12, Nov. 2010, Art. no. 125016. doi: 10.1088/0960-1317/20/12/125016.

[13] A. Macor, E. de Rijk, S. Alberti, T. Goodman, and J.-P. Ansermet, "Note: Three-dimensional stereolithography for millimeter wave and terahertz applications," *Rev. Sci. Instrum.*, vol. 83, no. 4, Apr. 2012, Art. no. 046103.

[14] (Mar. 23, 2018). *ANSYS HFSS, Release 2015.2.0.* [Online]. Available: https://www.ansys.com/products/electronics/ansys-hfss

[15] A. von Bieren, E. de Rijk, J.-P. Ansermet, and A. Macor, "Monolithic metal-coated plastic components for mm-wave applications," in *Proc. 39th Int. Conf. Infr., Millim., THz. Waves (IRMMW-THz)*, Tucson, AZ, USA, Sep. 2014, pp. 1–2. doi: 10.1109/IRMMW-THz.2014.6956222.

[16] A. R. Gans, M. M. Jobbins, D. Y. Lee, and S. A. Kandel, "Vacuum Compatibility of silver and titanium parts made using three-dimensional printing," *J. Vac. Sci. Technol. A, Vac. Surf. Films*, vol. 32, no. 2, p. 023201, Mar. 2014. doi: 10.1116/1.4846195.

[17] A. P. Povilus, C. J. Wurden, Z. Vendeiro, M. Baquero-Ruiz, and J. Fajans, "Vacuum compatibility of 3D-printed materials," *J. Vac. Sci. Technol. A, Vac. Surf. Films*, vol. 32, no. 3, May 2014, Art. no. 033001. doi: 10.1116/1.4873556.

[18] N. M. Jordan, G. B. Greening, S. C. Exelby, R. M. Gilgenbach, Y. Y. Lau, and B. W. Hoff, "Additively manufactured anodes in a relativistic planar magnetron," in *Proc. IEEE Int. Vac. Electron. Conf. (IVEC)*, Monterey, CA, USA, Apr. 2016, pp. 1–2. doi: 10.1109/IVEC.2016.7561848.

[19] A. M. Cook, C. D. Joye, R. L. Jaynes, and J. P. Calame, "W-band TWT circuit fabricated by 3D-printed mold electroforming," in *Proc. IEEE Int. Vac. Electron. Conf. (IVEC)*, Monterey, CA, USA, pp. 331–332, Apr. 2018. doi: 10.1109/IVEC.2018.8391511.

ALAN M. COOK (M'07–SM'16) received the Ph.D. degree in physics from the University of California at Los Angeles, in 2009. He completed his Postdoctoral work at the Plasma Science and Fusion Center, Massachusetts Institute of Technology. He joined the Naval Research Laboratory, Washington, DC, USA, in 2011. His research interests include microfabrication methods, materials, and device design for upper-millimeter-wave vacuum electron devices.

COLIN D. JOYE (M'03–SM'13) received the Ph.D. degree from the Massachusetts Institute of Technology, in 2008. He joined the Naval Research Laboratory, Washington, DC, USA, in 2008. His research interests include microfabrication technologies for millimeter- and submillimeter-wave vacuum electronics.

JEFFREY P. CALAME (M'96–SM'11–F'18) received the Ph.D. degree in electrical engineering from the University of Maryland, College Park, MD, USA, in 1991. He has been with the Naval Research Laboratory, Washington, DC, USA, since 1997. His research interests include microwave and millimeter-wave amplifiers, as well as dielectric and composite materials, metamaterials, energy storage, high-heat-flux thermal management, and microfabrication.